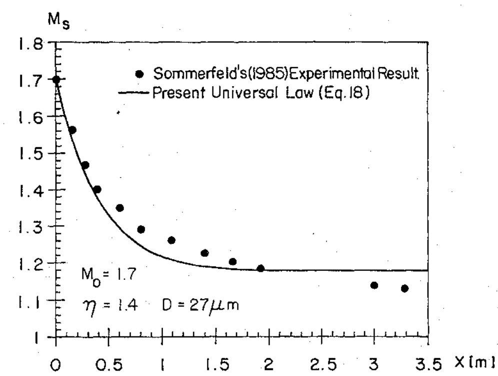

Fig. 1 Comparison between the attenuation predicted by the general attenuation law developed in the course of the present study and the experimental results of Sommerfeld.[3]

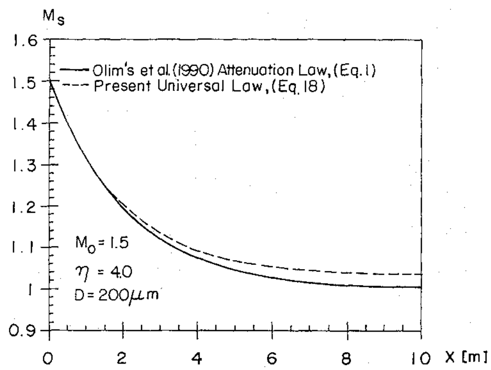

Fig. 2 Comparison between the predictions of the attenuation laws developed during the course of the present study (dashed line) and that developed by Olim et al.[1]

as mentioned earlier is applicable only to weak-to-moderate planar shock waves and relatively high loading ratios, is shown in Fig. 2 for $M_0 = 1.5$, $D = 200\ \mu$m, and $\eta = 4.0$. It is evident that the general attenuation law as developed in the course of the present study predicts an attenuation similar to that predicted by Olim et al.'s[1] limited law. The difference of about 3 to 4%, which is developed at large values of x, is due to the fact that whereas the present general attenuation law dictates a realistic equilibrium shock wave Mach number, $M_e \geq 1$, Olim et al's[1] specific attenuation law inherently dictates $M_e = 1$ when $x \to \infty$.

Conclusions

The governing equations describing the flowfield that develops when a planar shock wave propagates inside a dust-gas suspension were solved numerically using the random choice method.

The shock wave attenuation was investigated numerically. Based on the numerical results, a general law for describing the shock wave attenuation as it propagates inside the dust-gas suspension was developed. It is an improvement of a simplified specific attenuation law that was developed a few years ago by Olim et al.[1] The results indicated that the coefficient of attenuation χ decreases as the dust particles diameter D decreases and the dust loading ratio η increases. As a result the attenuation itself increases when D decreases and η increases.

The general attenuation law was validated by comparing its prediction with actual experimental results. Very good agreement was evident.

The general attenuation law enables one to calculate simply and cheaply the instantaneous shock wave Mach number and as a result to obtain immediately the jump conditions across it without the need to conduct a tedious numerical simulation.

Acknowledgment

This research was supported by a grant from the German–Israeli Foundation for Scientific Research and Development. Their support is acknowledged with thanks.

References

[1]Olim, M., Ben-Dor, G., Mond, M., and Igra, O., "A General Attenuation Law of Moderate Planar Shock Waves Propagating into Dusty Gases with Relatively High Loading Ratios of Solid Particles," *Fluid Dynamics Research*, Vol. 6, No. 3–4, 1990, pp. 185–200.

[2]Sommerfeld, M., "Instationäre Stosswellenausbreitung in Gas-Teilchen-Gemiscen," Ph.D. Thesis, Faculty of Mechanical Engineering, Reinische-Westfälische Technische Hochschule Aachen, Aachen, Germany, 1984.

[3]Sommerfeld, M., "The Unsteadiness of Shock Waves Propagating through Gas-Particle Mixtures," *Experiments in Fluids*, Vol. 3, 1985, pp. 197–206.

[4]Boris, J. P., and Book, D. L., "Flux-Corrected Transport. I. SHASTA, A Fluid Transport Algorithm That Works," *Journal of Computational Physics*, Vol. 11, 1973, p. 38.

[5]Book, D. L., Boris, J. P., and Hain, K., "Flux-Corrected Transport. II. Generalization of the Method," *Journal of Computational Physics*, Vol. 18, 1975, pp. 248–283.

[6]Glimm, J., "Solution in the Large for Nonlinear Hyperbolic System Equations," *Communications in Pure and Applied Mathematics*, Vol. 18, 1965, pp. 95–105.

[7]Sod, G.A., "A Numerical Study of a Converging Cylindrical Shock," *Journal of Fluid Mechanics*, Vol. 83, 1977, pp. 785–794.

[8]Aizik, F., "Investigation of the Attenuation of Planar Shock Waves Propagating into Dusty Gases," M.Sc. Thesis, Dept. of Mechanical Engineering, Ben-Gurion Univ. of the Negev, Beer Sheva, Israel, 1992 (in Hebrew).

[9]Clift, R., Grace, J. R., and Weber, M. E., *Bubbles, Drops and Particles*, Academic, New York, 1978.

[10]Rudinger, G., "Effective Drag Coefficient for Gas-Particle Flow in Shock Tubes," *ASME Journal of Basic Engineering*, Vol. D92, 1970, pp. 165–172.

[11]Gilbert, M., Davis, L., and Altman, D., "Velocity Lag of Particles in Lineary Accelerated Combustion Gases," *Jet Propulsion*, Vol. 25, 1955, pp. 26–30.

[12]Bailey, A. B., "Sphere Drag Coefficient for Subsonic Speeds in Continuum and Free Molecule Flows," *Journal of Fluid Mechanics*, Vol. 65, 1974, pp. 401–410.

[13]Igra, O., and Takayama, K., "Shock Tube Study of the Drag Coefficient of a Sphere in a Non-Stationary Flow," *Proceedings of the Royal Society of London*, Series A, Vol. 442, 1993, pp. 231–247.

[14]Drake, R. M., "Discussion on the Paper Entitled 'Forced Convection Heat Transfer from an Isothermal Sphere to Water' by G. C. Violet and G. Leppert," *ASME Journal of Heat Transfer*, Vol. 83, 1961, pp. 170–175.

Interaction of a Regular Reflection with a Compressive Wedge: Analytical Solution

H. Li* and G. Ben-Dor†
Ben-Gurion University of the Negev,
Beer Sheva 84105, Israel

Introduction

An experimental and analytical study of the reflection processes of planar shock waves over double wedges was presented in Ref. 1. One out of the seven investigated double wedge combinations is shown in Fig. 1. The slopes of the first and second reflecting surfaces are θ_w^1 and θ_w^2, respectively, and θ_w^1 is large enough to ensure that the incident planar shock wave reflects over it as a regular reflection (RR). The case for which $\theta_w^2 < 90$ deg was investigated experimentally in Ref. 1 and numerically in Ref. 2, and the case

Received March 25, 1994; revision received Aug. 8, 1994; accepted for publication Aug. 15, 1994.

*Ph.D. Student, Pearlstone Center for Aeronautical Engineering Studies, Department of Mechanical Engineering.

†Professor and Dean, Faculty of Engineering Sciences, Pearlstone Center for Aeronautical Engineering Studies, Department of Mechanical Engineering.

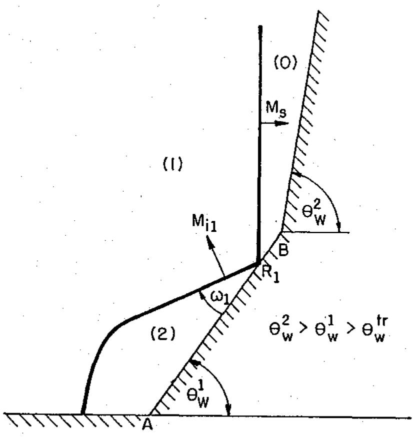

Fig. 1 Schematic illustration of a regular reflection prior to its interaction with a compressive corner and definition of parameters.

for which $\theta_w^2 = 90$ deg was investigated both experimentally and numerically in Ref. 3.

Schematic illustrations of the resulted wave configurations following the interactions of the regular reflections, which were formed over the first reflecting surfaces, with the second compressive corners for $\theta_w^2 < 90$ deg and $\theta_w^2 = 90$ deg are shown in Figs. 2a and 2b, respectively. The similarity between these wave configurations is self-explanatory. They both consist of two triple points, T_1 and T_2. As long as the signals generated at the first compressive corner (not shown in Fig. 2) have not reached the triple point T_1, the wave configurations shown in Figs. 2a and 2b are self-similar.[3]

In the following an analytical model based on the two- and three-shock theories for predicting the wave configurations, shown in Figs. 2a and 2b, respectively, is presented. Predictions based on the proposed analytical model are then compared to experimental results.

By comparing the analytical predictions with experimental results, the performance of the two- and three-shock theories in complicated flowfields can be checked. In addition, these theories can be further used to calculate local pressures along the reflecting surfaces, especially at point B where the pressure is maximal. Such information may assist in preliminary design of structures which could be hit by blast waves.

Present Study

The two- and three-shock theories[4] are, in fact, the analytical models for describing the local flowfields in the vicinity of the reflection point of an RR and the triple point of a Mach reflection (MR). It is assumed in these theories that all of the discontinuities, i.e., shock waves and slipstreams, are straight and that the flowfields bounded by them are uniform. In accordance with these assumptions, the wave configurations shown in Figs. 2a and 2b are redrawn in Fig. 3a. The schematic wave configuration shown in Fig. 3a is rotated by 90 deg compared to its counterpart in Fig. 2 and all of the discontinuities in it are straight. An (x, y)-coordinate system is defined in Fig. 3a. The wave configuration consists of two triple points, T_1 and T_2. The triple points trajectory angles are χ_1 and χ_2, respectively. Each triple point has three shock waves, namely, the incident i, the reflected r, and the Mach stem m, and one slipstream s. The Mach stem is common to the two triple points. An arrow indicating the direction of propagation is attached to each shock wave. The flow Mach number in region (j) is indicated as m_j. Note that m_1 is parallel to the y axis, m_2 is parallel to the first reflecting surface, and m_3 is parallel to the second reflecting surface. The incident, reflected, and Mach stem shock Mach numbers are M_{i_k}, M_{r_k}, and M_m, respectively, where the secondary subscript indicates the triple point to which the shock wave (i or r) belongs.

The flow parameters and representative streamlines in the vicinities of each of the two triple points in the frames of references attached to them are shown in Figs. 3b and 3c. To simplify the formulation in the following let us replace the notations of the first and second triple points from T_1 and T_2 to C and D, respectively. Furthermore, since dynamic properties are frame-of-reference dependent, the symbols (C) or (D) will be attached to them to indicate whether they are in a frame of reference attached to the first triple point C or the second triple point D. Whenever a dynamic property is not followed by (C) and (D) it is actually calculated in a laboratory frame of reference.

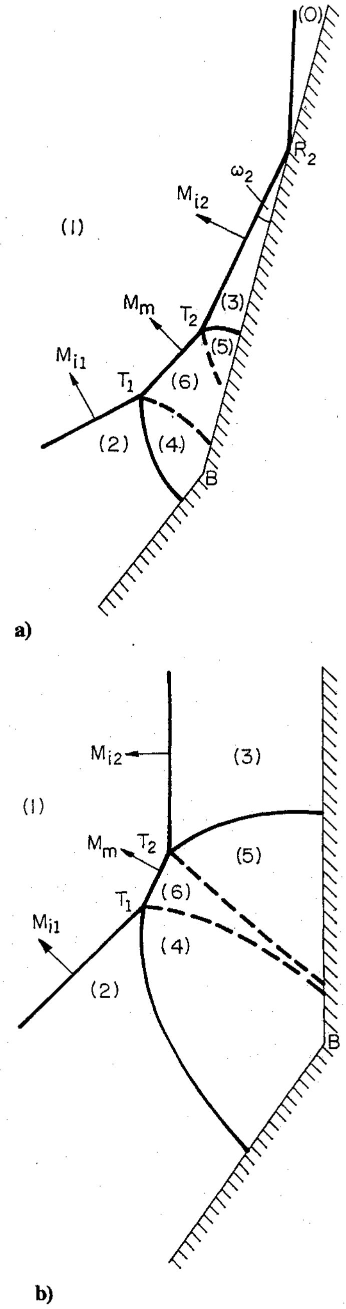

Fig. 2 Schematic illustrations of the wave configurations which are developed after the RR interacts with the compressive corner: a) $\theta_w^2 < 90$ deg and b) $\theta_w^2 = 90$ deg.

Governing Equations

Based on Fig. 3a the attachment velocity of the first triple point C is

$$v_C = \frac{M_{i1} - m_1 \sin\theta_1}{\cos(\chi_1 - \theta_1)} \cdot a_1 \tag{1}$$

where a is the local speed of sound, and θ_1 is defined in Fig. 3a. Let us define for this velocity two different Mach numbers

$$M_{Ci} = v_C / a_i \qquad i = 1, 2 \qquad \text{(2) and (3)}$$

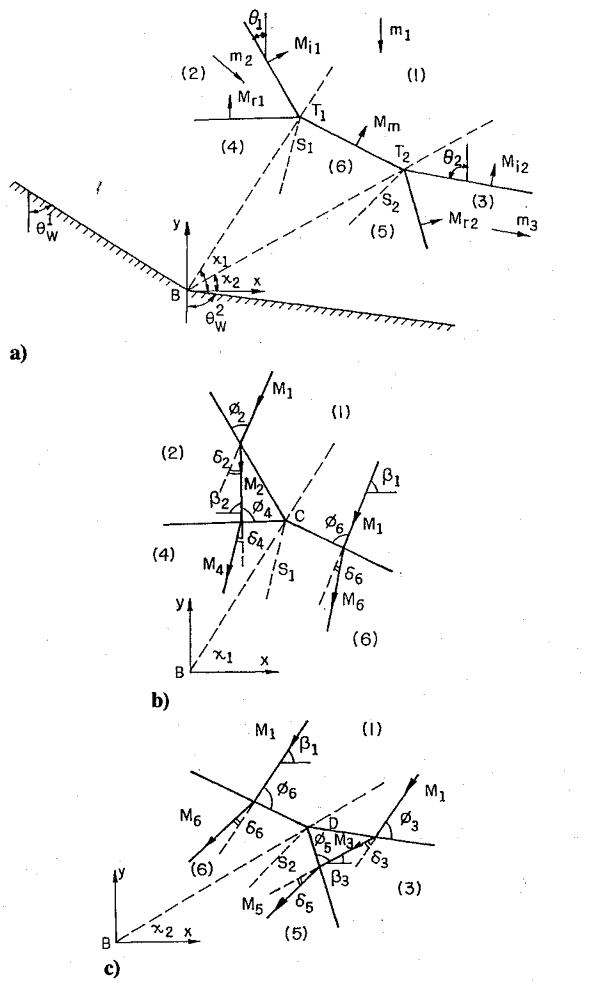

Fig. 3 Detailed schematic illustrations of the wave configurations shown in Fig. 2 with detailed definition of parameters.

Based on Fig. 3b and simple vector analysis one can write

$$M_1(C) = \left(M_{C1}^2 + m_1^2 + 2M_{C1}m_1 \sin\chi_1\right)^{\frac{1}{2}} \tag{4}$$

$$M_2(C) = \left[M_{C2}^2 + m_2^2 + 2M_{C2}m_2 \sin\left(\chi_1 - \theta_w^1\right)\right]^{\frac{1}{2}} \tag{5}$$

$$\beta_1(C) = \operatorname{arctg}\left(\frac{M_{C1}\sin\chi_1 + m_1}{M_{C1}\cos\chi_1}\right) \tag{6}$$

$$\beta_2(C) = \operatorname{arctg}\left(\frac{M_{C2}\sin\chi_1 + m_2\cos\theta_w^1}{M_{C2}\cos\chi_1 - m_2\sin\theta_w^1}\right) \tag{7}$$

From gas dynamic considerations one obtains

$$\delta_i(C) = \operatorname{arctg}\left\{2\operatorname{ctg}\phi_i(C)\frac{[M_j(C)\sin\phi_i(C)]^2 - 1}{M_j^2(C)[\gamma + \cos 2\phi_i(C)] + 2}\right\} \qquad \text{(8) and (9)}$$

$$p_i(C) = p_j(C)\frac{2\gamma[M_j(C)\sin\phi_i(C)]^2 - (\gamma - 1)}{\gamma + 1} \qquad \text{(10) and (11)}$$

where $i = 4$ and 6 for $j = 2$ and 1, respectively. In addition,

$$M_m = M_1(C)\sin\phi_6(C) \tag{12}$$

$$\theta_m = \beta_1(C) + \phi_6(C) - (\pi/2) \tag{13}$$

where M_m and θ_m are the strength and orientation of the Mach stem.

The matching conditions across the slipstream s_1 are

$$p_4(C) = p_6(C) \tag{14}$$

$$\beta_2(C) - \delta_4(C) = \beta_1(C) + \delta_6(C) \tag{15}$$

In addition, since the tangential velocity across oblique shock waves remains constant,

$$m_2 = \frac{m_1\cos\theta_1}{\cos\omega_1}\frac{a_1}{a_2} \tag{16}$$

Equations similar to Eqs. (1–16) can be derived for the second triple point D.

Based on Fig. 3a the attachment velocity of the second triple point D is

$$v_D = \frac{M_{i2} - m_1\sin\theta_2}{\cos(\chi_2 - \theta_2)}\cdot a_1 \tag{17}$$

where θ_2 is defined in Fig. 3a. Let us again define two different Mach numbers for this velocity

$$M_{Di} = v_D/a_i \qquad i = 1, 3 \qquad \text{(18) and (19)}$$

Based on Fig. 3c and simple vector analysis one can write:

$$M_1(D) = \left(M_{D1}^2 + m_1^2 + 2M_{D1}m_1\sin\chi_2\right)^{\frac{1}{2}} \tag{20}$$

$$M_3(D) = \left[M_{D3}^2 + m_3^2 + 2M_{D3}m_3\sin\left(\chi_2 - \theta_w^2\right)\right]^{\frac{1}{2}} \tag{21}$$

$$\beta_1(D) = \operatorname{arctg}\left(\frac{M_{D1}\sin\chi_2 + m_1}{M_{D1}\cos\chi_2}\right) \tag{22}$$

and

$$\beta_3(D) = \operatorname{arctg}\left(\frac{M_{D3}\sin\chi_2 + m_3\cos\theta_w^2}{M_{D3}\cos\chi_2 - m_3\sin\theta_w^1}\right) \tag{23}$$

From gas dynamic considerations one obtains

$$\delta_i(D) = \operatorname{arctg}\left\{2\operatorname{ctg}\phi_i(D)\frac{[M_j(D)\sin\phi_i(D)]^2 - 1}{M_j^2(D)[\gamma + \cos 2\phi_i(D)] + 2}\right\} \qquad \text{(24) and (25)}$$

$$p_i(D) = p_j(D)\frac{2\gamma[M_j(D)\sin\phi_i(D)]^2 - (\gamma - 1)}{\gamma + 1} \qquad \text{(26) and (27)}$$

where $i = 5$ and 6 for $j = 3$ and 1, respectively. In addition,

$$M_m = M_1(D)\sin\phi_6(D) \tag{28}$$

$$\theta_m = \beta_1(D) - \phi_6(D) + (\pi/2) \tag{29}$$

The matching conditions across the slipstream s_2 are

$$p_5(D) = p_6(D) \tag{30}$$

$$\beta_3(D) + \delta_5(D) = \beta_1(D) - \delta_6(D) \tag{31}$$

In addition, since the tangential velocity across oblique shock waves remains constant,

$$m_3 = \frac{m_1\cos\theta_2}{\cos\omega_2}\frac{a_1}{a_3} \tag{32}$$

Table 1 Comparison between analytical predictions and experimental results

	Case 1, $M_s = 1.25, \theta_w^1 = 55$ deg, $\theta_w^2 = 90$ deg		Case 2, $M_s = 1.49, \theta_w^1 = 55$ deg, $\theta_w^2 = 90$ deg	
	Analysis	Experiment	Analysis	Experiment
χ_1, deg	57.6	52 deg ±1	56.9	52 deg ±1
χ_2, deg	39.1	44 deg ±1	34.7	37.5 deg ±1
θ_m, deg	56.6	56 deg ±1	58.4	58 deg ±1

The set of 32 governing equations consists of the following 32 unknowns: v_C, M_{C1}, M_{C2}, $M_1(C)$, $M_2(C)$, $\beta_1(C)$, $\beta_2(C)$, $\delta_4(C)$, $\delta_6(C)$, $p_4(C)$, $p_6(C)$, M_m, θ_m, m_2, $\phi_4(C)$, $\phi_6(C)$, χ_1, v_D, M_{D1}, M_{D2}, $M_1(D)$, $M_3(D)$, $\beta_1(D)$, $\beta_3(D)$, $\delta_5(D)$, $\delta_6(D)$, $p_5(D)$, $p_6(D)$, m_3, $\phi_5(D)$, $\phi_6(D)$ and χ_2.

Note that the speed of sound a_1 behind the incident shock wave is simply obtained from M_s and a_0. The parameters M_{i1}, θ_1, a_2, and ω_1 can be obtained from solving the regular reflection of incident shock wave M_s over the first reflecting surface θ_w^1. Similarly, M_{i2}, θ_2, a_3, and ω_2 can be obtained from solving the regular reflection of the incident shock wave M_s over the second reflecting surface θ_w^2. Recall that M_s, θ_w^1, θ_w^2, and the flow state (0) are all known, as they are the initial conditions.

Results and Discussion

Predictions of the proposed analytical model were compared with the relevant experimental results of Refs. 1–3. Three geometrical parameters were compared: the first and second triple point trajectory angles χ_1 and χ_2 and the orientation of the Mach stem θ_m with respect to the horizontal x axis. The comparison is shown in Table 1. Whereas the analytical predictions of χ_1 overestimate the experimental results by about 10%, the analytical predictions of χ_2 underestimate the experimental results by about 10%. Although these agreements do not seem to be too good, one should recall that similar agreement is obtained when the three-shock theory is used to predict the triple-point trajectory angle in Mach reflections over single wedges.[4] The reason for this disagreement lies in the fact that in actual triple points not all of the shock waves are straight as required by the two- and three-shock theories. Figures 2a and 2b clearly indicate this fact. Furthermore, whereas in the case of single wedges the triple point moves toward a quiescent gas in the wave configuration treated in the present study, the triple points move toward a moving gas. Consequently, the present problem is much more complicated and, hence, an agreement within 10% should practically be considered as a very good one. Finally, it should be noted that as is evident from Table 1, the agreement between the presently proposed analytical model and the experimental results, regarding the orientation of the Mach stem, i.e., θ_m, is excellent.

Conclusions

The two- and three-shock theories were applied to complex flowfields and wave structures. Their performance was found to be good to excellent. By further developing this model the pressures acting on the surfaces can be estimated.

References

[1]Ben-Dor, G., Dewey, J. M., and Takayama, K., "The Reflection of a Plane Shock Wave Over a Double Wedge," *Journal of Fluid Mechanics*, Vol. 176, 1987, pp. 483–520.

[2]Itoh, K., Takayama, K., and Ben-Dor, G., "Numerical Simulation of the Reflection of a Planar Shock Wave Over a Double Wedge," *International Journal of Numerical Methods in Fluids*, Vol. 13, 1991, pp. 1153–1170.

[3]Falcovitz, J., Alfandary, G., and Ben-Dor, G., "Numerical Simulation of the Head-On Reflection of a Regular Reflection," *International Journal of Numerical Methods in Fluids*, Vol. 17, 1993, pp. 1055–1078.

[4]Ben-Dor, G., *Shock Wave Reflection Phenomena*, Springer-Verlag, New York, 1991, Chap. 1.

Effect of Screen Porosity and Location on Wind-Tunnel Turbulence

G. Refai Ahmed* and E. Brundrett†
University of Waterloo, Waterloo, Ontario N2L 3G1, Canada

Introduction

ONE of the fundamental problems of engineering fluid mechanics is how to control the velocity distribution of fluid flow inside the wind tunnel. Often, single screen or multiple screens are used in this operational mode to remove or create time-mean velocity nonuniformities and to reduce or increase the intensity of turbulence in a controlled manner. Numerous studies have investigated the effect of placing screens in the fluid flow through wind tunnels since the beginning of this century. Furthermore, the researchers have examined the effect of the turbulence intensity, as controlled by the screens, on forced convection heat transfer results.

A wide variety of turbulence generators have been examined in the past, such as square-mesh arrays of either round rods or wires (woven screens), square-mesh arrays of square bars, parallel arrays of square bars, perforated plates, agitated bar grids, jet grids, aerofoil cascades, tube bundles, and various permutations and combinations of the preceeding. Roach[1] investigated the pressure drop across screens and the characteristics of the downstream turbulence. Furthermore, Roach[1] attempted to fill gaps in the current literature by proposing simple rules for the design of screens in wind tunnels. Therefore, he proposed design guidelines and also examined the pressure losses, turbulence intensities, spectra, correlation functions and length scales. In addition, Roach[1] introduced a number of correlations to predict turbulence intensity behind a screen; however, he did not address the effect of screen porosity on turbulence intensity. Laws and Livesey[2] investigated the flow through screens by characterizing the flow properties of the screen, by determining the effect of a screen on time-mean velocity distributions, and by measuring the turbulence distribution downstream of gauze screens. Furthermore, Gad-el-Hak and Corrsin[3] gave details of turbulence intensities, scales, decays, and spectra for their jet grid. In the same paper they summarized the results, in tabular form, of no less than 12 previous paper on both passive and active grids giving the turbulence component magnitudes and decays of the form

$$\cot u/u \times 100Tu = B(x/M)^{-m} \tag{1}$$

where B and m are constants, x is the distance between the location of the screen and the measurement location of Tu, and M is square cell width of the screen based on wire centerline. Batchelor and Townsend[4] and Compte-Bellot and Corrsin[5] correlated their

Received April 4, 1994; revision received Sept. 15, 1994; accepted for publication Sept. 20, 1994.

*Graduate Research Assistant, Department of Mechanical Engineering. Senior Member AIAA.

†Professor, Department of Mechanical Engineering.